Materials Today Communications xxx (xxxx) xxx

Contents lists available at ScienceDirect

Materials Today Communications

journal homepage: www.elsevier.com/locate/mtcomm

Difference in lipid cell composition and shaped-based gold nanoparticles induce distinguish pathways in Langmuir monolayers response

J. Cancino-Bernardi *, P.M.P. Lins, V.S. Marangoni, H.A.M. Faria, V. Zucolotto

Nanomedicine and Nanotoxicology Group, Physics Institute of São Carlos, University of São Paulo, CP 369, 13560-970 São Carlos, São Paulo, Brazil

ARTICLE INFO

Keywords:
Membrane models
Nanotoxicology
Nanobiointerfaces
Nanoparticles
Nanorods

ABSTRACT

Understanding the interactions occurring at the nano-bio interface is still a challenge. This study presents an investigation on the interactions between natural cell membranes and gold-based particles that were isolated from real - cancer and health - cells and reconstructed as monolayers. The influence of the morphology and surface charge of gold nanomaterials on the membrane structure, as well as the interface properties of the membranes was evaluated. Our results revealed that the interaction pathway of nanoparticles through the cell membrane was affected by the lipidic composition of each cell type evaluated. Moreover, we show that the surface charge of the nanoparticles plays a significant role in their ability to interact with cell membranes, as revealed by isothermal titration calorimetry, and atomic force microscopy analysis.

1. Introduction

Bio-nano interfaces are of great importance for understanding the interactions of nanomaterials on biological systems and for predicting their adverse effects [1–6]. Because of thermodynamic changes that may occur between the nanomaterials surface and biological cell membrane components such as proteins, phospholipids and organelles, these interfaces can reveal important dynamic information about nanobio interactions [1,7]. The nanomaterial`s properties, including nanoparticle charge, size, surface area, functional groups, linkers, and hydrophilicity, are known to influence their interactions with biological molecules [8–10].

Another important feature regarding the interaction of nanomaterials with biomolecules is related to the solid–liquid interface. At this interface, nanoparticle–biomolecule interactions occur through specific and non-specific forces that exist between the membrane components and the nanoparticle surface. Phenomena occurring at this interface should be taken into account, such as the formation of a hydration layer from water molecules, ionic adsorption, development of an electric double-layer, and protein corona formation [5]. The solid–liquid interface is one of the major challenges in understanding the nano-bio interactions. Most of the experiments described at literature are carried out under steady-state conditions, which differ from the dynamic behavior of biological systems [4,11]. Despite recent progress in understanding the interactions occurring on the cell surface, it is still difficult to predict the biological behavior and toxicity of nanoparticles due to the experimental limitations.

The characteristics of the cell membrane also play an important role at the solid–liquid interface between a cell and a nanoparticle. Healthy cells differentiated from the cancerous ones because of the translocation across the cancer cell membrane and also by cancer markers biomolecules [12,13]. The amount of each component in the cell membrane may vary on a large scale [14–16]. For example, cancer cell membranes are known to have many carbohydrates and disaccharide molecules which can create an asymmetry in the membrane and a surface layer that covers the entire outer surface of the cell membrane, which in turn may generate an electrical potential on the cell surface because of the electrical charge accumulation [13,17]. These differences strongly affect the uptake of molecules and nanoparticles into or through the cell, altering the fluidity and dynamic arrangement of lipids in the membrane. The variations of surface charges influence the membrane curvature and packing density because of charge–charge repulsion from the polar head group of the lipids, affecting the physiology of the membrane as a consequence of impermeability changes [16,18].

Some of the changes in the molecular arrangement of the phospholipids can be monitored *via* the Langmuir monolayer technique, which measures the surface potential from the air–water interface of the dipole moment of the molecules. The transition phase is quite dependent on the

* Corresponding author at: Nanomedicine and Nanotoxicology Group, Physics Institute of São Carlos, University of São Paulo, Avenida São-carlense, 400, CP 369, CEP: 13560-970 São Carlos, São Paulo, Brazil.
E-mail address: jcancinobernardi@gmail.com (J. Cancino-Bernardi).

https://doi.org/10.1016/j.mtcomm.2020.101831
Received 2 July 2020; Received in revised form 29 September 2020; Accepted 25 October 2020
Available online 2 November 2020

interactions of the polar groups of the lipids and the orientation of their carbon chains. Investigating bio-nano interfaces on a molecular level is possible by controlling the lipid composition and their transition phases. Membrane models are simplified systems in which some physical and chemical interface parameters can be controlled to reveal monolayer formation, the molecular area compressibility of the interface, and the interactions between molecules in the monolayer in terms of their subphases and stability [11,19,20]. Evidence of monolayers and nanoparticles interaction have been reported using synthetic phospholipids molecules [21–26].

To understand the influence of cell membrane composition in the uptake of nanomaterials, cell membranes from F C3H (normal fibroblasts from the liver) and HTC (hepatoma epithelial cells from the liver) were extracted, characterized, and reconstructed at the Langmuir trough. Some changes were observed in relation to the pressure and surface tension of these monolayers in the presence or absence of nanoparticles, which revealed possible interactions occurring at the bio-nano interface. The influence of morphology and surface charge of gold nanostructures including gold nanoparticles (AuNPs), positively charged gold nanorods (AuNRs), and polyethylene glycol (PEG)-coated AuNRs were compared regarding their abilities to interact with membranes from F C3H and HTC. To further understand these interactions, isotherm titration calorimetry (ITC) measurements, and atomic force microscopy (AFM) images were also performed.

2. Methods

2.1. Synthesis of gold nanoparticles and gold nanorods

The synthesis of AuNPs coated with poly(allylamine hydrochloride) (PAH) average M_W 50,000 was performed using the chemical reduction of gold ions in the presence of the polymer. Briefly, 20 mL of 1 mg mL^{-1} PAH was mixed with 20 mL of 1 mmol L^{-1} $HAuCl_4$ under gentle stirring. Then, 1 mL of a 0.01 mol L^{-1} $NaBH_4$ solution was added and the system was vigorously stirred for 30 min. The suspension was then left to rest at room temperature and protected from light to allow the particle growth. Finally, the nanoparticles were washed by centrifugation at 10,000 *g* for 15 min to remove the excess polymer and the resulting pellet was resuspended in ultrapure water.

Gold nanorods were synthetized based on the seed-growth method in the presence of the surfactant cetyltrimethylammonium bromide (CTAB) [36]. First, 7.5 mL of 0.1 mol L^{-1} CTAB was mixed with 250 mL of 0.01 mol L^{-1} $HAuCl_4$ under stirring for 1 min. Then, 600 µL of cold 0.01 mol L^{-1} $NaBH_4$ solution was added under vigorous stirring. After 10 min, the color of the solution changed from yellow to pale brown. This suspension was then kept at 25 °C for 2–3 h before use. Growth of the NRs was performed by mixing 3 mL of 0.01 mol L^{-1} $HAuCl_4$ with 47 mL of 0.1 mol L^{-1} CTAB, followed by the addition of 350 mL of 0.01 mol L^{-1} $AgNO_3$ and 480 µL of 0.1 mol L^{-1} ascorbic acid. Finally, 100 µL of the previously prepared gold seeds were added. The system was kept at room temperature for at least 12 h and then centrifuged at 1500 *g* for 2 min to remove excess crystallized CTAB. The supernatant was centrifuged at 8000 *g* for 5 min. The resulting pellet was resuspended in ultrapure water. This centrifugation process was repeated twice to ensure the elimination of the excess of CTAB.

The nanorod surface was further modified with the polymers PAH and PEG. For this, the CTAB was removed by mixing the nanorods with chloroform and stirring vigorously for 15 min. The system was kept undisturbed to allow phase separation. The aqueous phase containing the nanorods was collected and analyzed by zeta potential to ensure that CTAB was majoritary removed. The nanorods were then immediately mixed with the same volume of a 1 mg mL^{-1} PAH or PEG solution under constant stirring for 12 h. Finally, the system was washed twice by centrifugation at 8000 *g* for 5 min and then resuspended in ultrapure water.

The concentration of the resulting PAH or PEG-coated AuNRs for the experiments were standardized by their optical density at the longitudinal absorption and their extinction cross section.

The morphology and sizes of the particles were determined by transmission electron microscopy (JEOL JEM-2100, 200 kV). Particles were further characterized by ultraviolet–visible–near infrared (UV–vis–NIR) spectroscopy (Hitachi U-2900). Dynamic light scattering and the surface charges of the particles were peeformed in triplicate at room temperature using Nano-ZS, Malvern Instruments. The zeta potential measurements of the PAH or PEG-coated AuNRs were evaluated in ultrapure water pH = 5,5.

2.2. Membrane extraction protocol

The next steps were performed on ice or at 4 °C and all buffers contained complete protease inhibitor (Roche).

F C3H and HTC cell lines supplied by Cell Bank Rio de Janeiro (Rio de Janeiro, Brazil) were used for the *in vitro* experiments. Each cell line (1×10^5 mL) was incubated in Dulbecco's Modified Eagle's Medium (DMEM) culture medium with 10 % bovine serum in 5 % CO_2 atmosphere at 37 °C. The medium was renewed 1–2 times per week with a subcultivation ratio of 1:2 to 1:4. Cell growth was monitored using a Zeiss microscope with a 10× objective. All processes were performed in a laminar flow hood. It is important note that F C3H is a primary cell line obtained from a normal adult C3H/Hej mouse according to Cell Bank Rio de Janeiro - Brazil specifications and its most used name is C3H/He.

Cells were removed from the flasks (total of $\sim 4 \times 10^7$ cells = 2 flasks of 75 cm^2), followed by two rounds of washing in phosphate buffered saline (PBS). They were incubated in a lysis buffer (255 mM sucrose), 20 mM 4-(2-Hydroxyethyl)piperazine-1-ethanesulfonic acid (HEPES), 1 mM (Ethylenedinitrilo)tetraacetic acid (EDTA) pH 7.4 and homogenized using a tip sonicator for 10 min at 25 % amplitude, followed by sedimentation by centrifugation at 300 *g* and 4 °C for 10 min. The supernatant was centrifuged at 10.000 *g* for 20 min to remove cell debris and nuclei. The supernatant was further centrifuged at 100.000 *g* for 2 h using an ultracentrifugation process. In order to eliminate protein complexes, the pellet fraction was resuspended in a 40 % sucrose cushion solution with a density of 1.12 g/mL and the the solution was ultracentrifuged at 100.000 *g* for additional 2 h. Although high-density extracellular vesicles infiltrated the cushion during subsequent ultracentrifugation, proteins remained in the supernatant. The pellet, which contained the crude membrane, was resuspended in PBS buffer and sedimented using the same ultracentrifugation conditions. Finally, the pellet was resuspended in PBS. The cell membrane purification process, adapted from Ref. [27], is summarized in Scheme 1. An aliquot was collected after each step for analysis, as illustrated below.

2.3. Membrane characterization

BCA protein assay was performed according the Pierce™ BCA Protein Assay Kit instructions from Thermo Fisher Scientific. This method combines the well-known reduction of Cu^{+2} to Cu^{+1} by protein in an alkaline medium (the biuret reaction) with the highly sensitive and selective colorimetric detection of cuprous cations (Cu^{+1}) using a unique reagent containing bicinchoninic acid. The purple-colored reaction product of this assay is formed by the chelation of two molecules of BCA with one cuprous ion, and it exhibits a strong absorbance at 562 nm that is nearly linear with increasing protein concentration over a broad working range (20–2000 µg/mL). Each standard or unknown sample (25 µL) was replicated into a microplate well (working range = 20–2000 µg/mL). The working reagent (200 µL) was added to each well and the plate was mixed thoroughly on a plate shaker for 30 s. The plate was then covered and incubated at 37 °C for 30 min. The plate was cooled to room temperature and the absorbance near 562 nm was read using a microplate reader spectrophotometer.

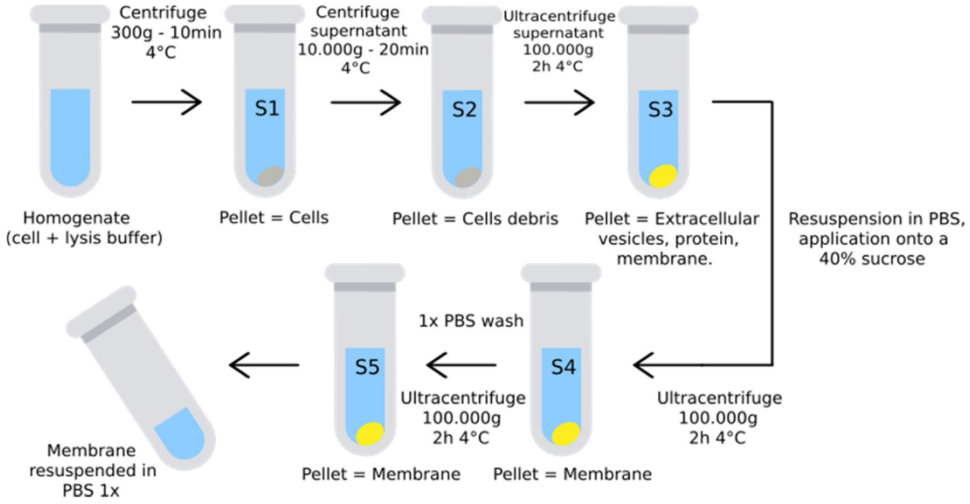

Scheme 1. Schematic of the cell membrane protocol used in this work. The protocol was adapted from Ref. [27].

2.4. Langmuir monolayers

Surface pressure per area (and time) measurements were performed using a mini-Langmuir trough from KSV-Nima Technology Ltd., which was made from poly(tetrafluoroethylene) and equipped with two barriers of the same material. The maximum surface area of the trough is 98.000 mm^2. The surface pressure was measured with a Wilhelmy plate of wet filter paper suspended from a strain gauge. Before spreading the lipids, the surface of the trough was cleaned with chloroform and then with ethanol followed by water to remove any excess solvent. Subphase solutions with or without nanoparticles were added to the trough and the temperature was maintained at 21 ± 1 °C. The monolayers were produced by spreading 6 μL of the F C3H or HTC membrane samples diluted in chloroform:methanol using a Hamilton syringe. These monolayers were allowed to reach equilibrium for 2 h before compression. In the hysteresis experiments, the barriers were compressed and decompressed at a rate of 10 mm min^{-1} until the surface pressure reached 50 mN m^{-1}, for 6 successive cycles. F C3H and HTC monolayers were investigated in presence of AuNP (~6 × 10^{11} particles/mL) and AuNR and AuNR-PEG concentrations of approximately 2 × 10^{12} particles/mL. In order to analyze the *in-situ* interaction of the F C3H and HTC monolayers and nanoparticles, 2 h adsorption kinetics were performed on expanded monolayers, followed by compression–decompression experiments. Langmuir monolayers where chosen as suitable technique to try understand the molecular interface between extracted lipids and nanoparticles, it means that the differences in lipid behavior as used to observe such effect. Although their extensively use, Langmuir results does not provide any information about the curvature effect or membrane-biomolecules activeness due to their experimental and theoretical limitations, in this case, other techniques should be included together to evaluated these effects.

2.5. Isothermal calorimetry titration (ITC)

All ITC experiments were performed with a MicroCal 200 instrument. The gold nanorods were titrated into a membrane in a buffer solution (1 mM Tris−HCl, pH = 7.4) at 25 °C. The first injection was 0.4 μL, followed by a series of 2 μL injections. Control experiments were also carried out by titrating nanorods at the same concentration into the buffer. The concentration of nanorods used in these experiments was approximately 10^{-10} particles/mL of AuNR and 10^{-9} particles/mL of AuNR-PEG. The membrane was extracted as described above and resuspended in 200 μL of buffer solution. The nanorods were dialyzed 48 h prior the measurement to be in the same buffer as the extracted membranes. The final curves were obtained using Origin software supplied by Malvern.

2.6. Atomic force microscopy (AFM)

The samples from the ITC experiments and the samples of F C3H, HTC, AuNPs, and AuNRs were processed and investigated by AFM under the same conditions. To preserve the cells' morphologies, the samples were measured under humidity. For the imaging, 5 μL of the membrane suspension was dropped onto a freshly cleaved mica surface and left to dry for 2 h at 25 °C. The mica surface is used in membrane AFM imaging because of its hydrophilic character and atomic flatness. Images were collected using a FLEX-AFM atomic force microscope (Nanosurf, Switzerland) operated in intermittent contact mode. A silicon cantilever Tap300-G from Budget Sensors with a spring constant of 40 N/m was used. All experiments were performed at room temperature.

3. Results

Fig. 1(a–g) show the characterization of the AuNPs and AuNRs. According to the UV–vis spectra [Fig. 1(f)], the plasmon bands of the PAH or PEG-coated AuNRs exhibited a bands centered at 500 nm and 900 nm. The size and morphology of the AuNRs were confirmed by the TEM image [Fig. 1(a)] and histograms [Fig. 1(b) and (c)], which revealed transversal and longitudinal sizes of 18.3 nm and 50.5 nm, respectively, with an aspect ratio (length/width) of approximately 2.8 nm. Meanwhile, the TEM image of the AuNPs showed the standard AuNP shape [Fig. 1(d)], and the particles had an average diameter of 14.4 nm according to Fig. 1(e). The surface charges of the nanoparticle and membrane samples were compared by zeta potential measurements [Fig. 1 (g)]. The zeta potential of the AuNPs and AuNRs was approximately +35 mV, suggesting stable and positively charged nanoparticles, whereas both membrane samples presented a negative surface charge of approximately −10 mV. Only the PEG-coated AuNRs were a closer to a neutral charge, approximately 9 mV.

The concentrations of cell membrane proteins were estimated by bicinchoninic acid (BCA) assay. The results indicated that 428 μg/mL and 590 μg/mL of protein was extracted from *ca.* 4 × 10^7 F C3H and HTC cells, respectively. Planar chromatography with flame ionization detection was used to characterize the lipid classes extracted from the F C3H and HTC membrane cells. Fig. 2(a–c) show the qualitative results of the lipid classes obtained from the samples.

From Fig. 2(a), six lipid class cell membranes extracted from F C3H cells are identified: approximately 3 % triglycerides (TAG), 11 % free fatty acids (FFA), 15 % free aliphatic alcohol (ALC), 2 % sterol (ST), 6 % mobile polar lipids in ketone (MPL), and 62 % phospholipids (PL). In

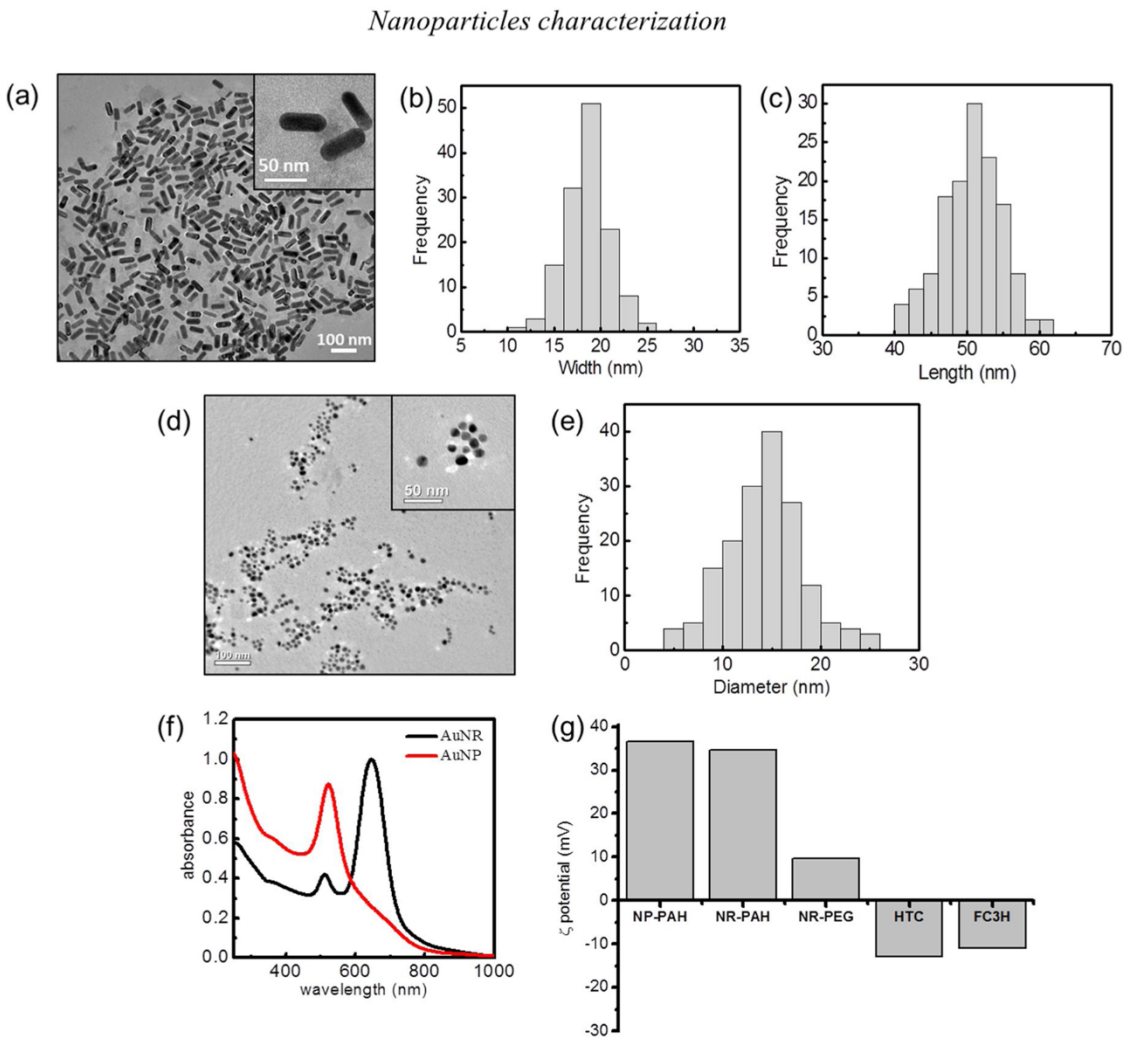

Fig. 1. TEM images and histograms of (a, b, c) AuNRs and (d, e) AuNPs determined by measuring approximately 150 particles using the software ImageJ. (f) UV–vis spectra and (g) zeta potential values of the AuNRs and AuNPs.

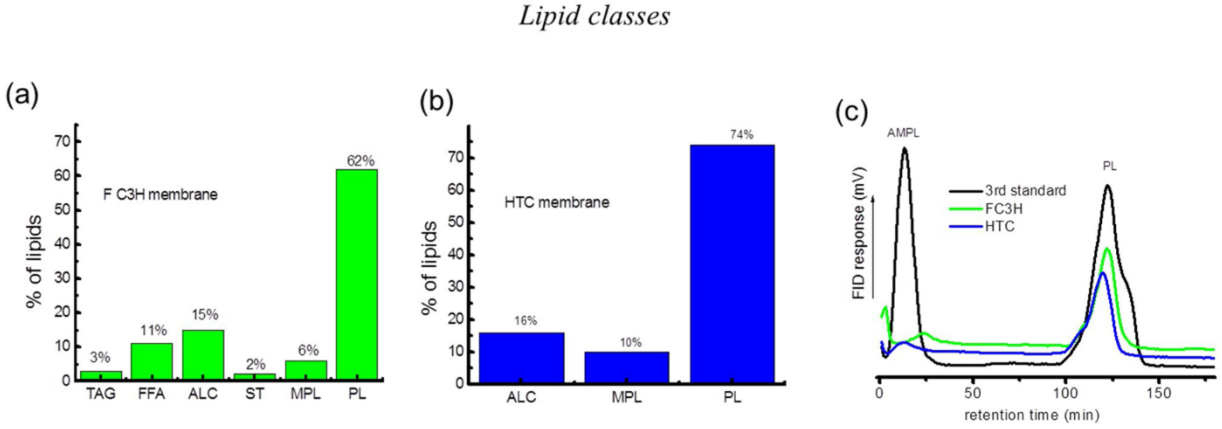

Fig. 2. Lipid classes: triglycerides (TAG), free fatty acids (FFA), free aliphatic alcohol (ALC), sterol (ST), mobile polar lipids in ketone (MPL), and phospholipids (PL) found in (a) F C3H and (b) HTC membrane samples. (c) Representative planar chromatogram from phospholipid (PL) class.

contrast, in HTC cell membranes, only three classes of lipids are identified: 16 % ALC, 10 % MPL, and 74 % PL (Fig. 2(b)). For both cells, phospholipids represent the majority [Fig. 2(c)], and it is in line with the literature, which reported at least 60 % phospholipids in an animal cell line [14].

Surface pressure was monitored as function of time to determine the minimum period necessary to obtain a stable monolayer. The kinetic profiles were observed for a period of 2 h to avoid evaporation of the subphase, which could affect the biointerface. Fig. 3(a) presents the kinetics graphs for the F C3H and HTC monolayers. While HTC forms a

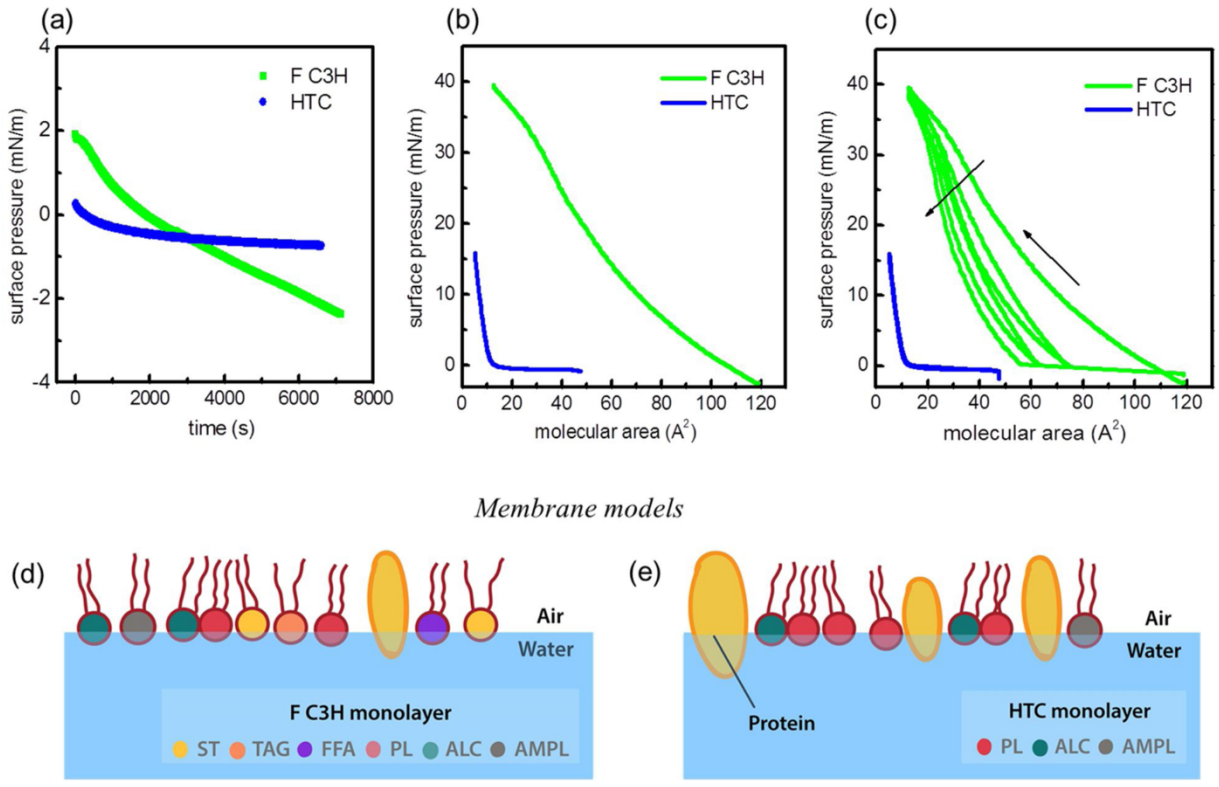

Fig. 3. (a) Adsorption kinetics graphs, (b) Langmuir isotherms, and (c) compression–decompression isotherm cycles of F C3H and HTC membranes cells as monolayers at the air–water interface. Lipid arrangement of the membrane samples as monolayers are illustrated in (d) and (e). Changes in the surface pressure *vs* time were monitored over 2 h.

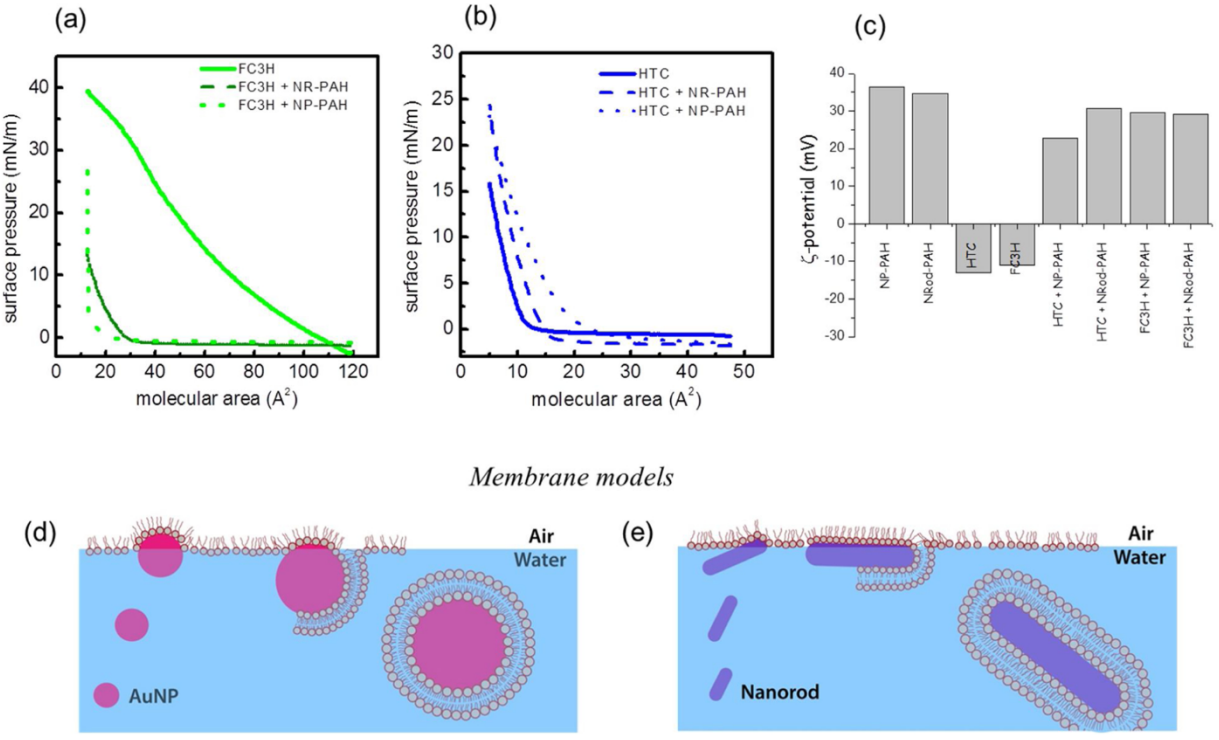

Fig. 4. Surface pressure–area isotherms of (a) F C3H and (b) HTC monolayers with AuNRs or AuNPs with ~10^9 particles/mL in the subphase. (c) Zeta potential values obtained from the subphase of the Langmuir trough containing nanoparticles after compression of the monolayer. Nanoparticle–lipid arrangements of membrane samples as monolayers are illustrated in (d) and (e).

stable monolayer right after its spreading on the water subphase, F C3H shows a decreasing of the surface pressure with time. The barriers were then closed at a rate of 10 mm min^{-1} to obtain a compressed monolayer, as observed in the Langmuir isotherms of Fig. 3(b). (c) shows the stability of both monolayers throughout the compression–decompression cycles. In the first cycle, the F C3H membrane was unstable during decompression, with a decrease in molecular area from 50 $Å^2$ to 40 $Å^2$ at a surface pressure of 20 mN/m. This decrease was more pronounced when the monolayer was subjected to multiple cycles, reaching a molecular area of 30 $Å^2$ at the same pressure. Based on that, one can illustrate the possible membrane arrangements [Fig. 3(d) and (e)].

Fig. 4(a) and (b) compares the surface pressure as function of molecular area for the F C3H and HTC monolayers in the presence and absence of the AuNRs and AuNPs. The surface pressure by time plots are presented in Fig.SI-1 and were used to evaluate changes in the isotherms and surface pressure profiles induced by the presence of the AuNRs and AuNPs in the subphase. Moreover, samples from the subphases containing the AuNR and AuNP particles were collected and their zeta potential values were measured to check possible interactions between both systems.

Fig. SI-1a shows that the F C3H monolayer presents the highest difference in surface pressure, from $\Delta\pi = 4$ mN/m to $\Delta\pi = 1$ mN/m after the introduction of either AuNPs or AuNRs into the subphase. This suggests that the F C3H monolayer was affected by the presence of nanoparticles, becoming apparently more stable over time. This was probably because of the existence of more apolar lipids in the F C3H membrane that were preferably organized at the subphase in the presence of the nanoparticles after their interaction. Similar behavior was observed in the HTC monolayer, as shown in Fig. SI-1b, although not to the same extent. Those effects are more noticeable in the isotherm results shown in Fig. 4(a) and (b).

The compression–decompression cycles were performed to check the particle/membrane interaction, and the results are shown in Fig. SI-2. To evaluate whether the charge of the nanoparticle coating has an influence in the interaction, we used PEG-coated gold nanorods (AuNR-PEG) and the results are shown in Fig. 5.

Fig. 5(a) and (b) show significant differences in the F C3H and HTC monolayers containing AuNR-PEG in the subphase compared to the AuNR-PAH. First, the kinetic process behavior (Fig. SI-3), which reveal an increase in the surface pressure with time, is the opposite of that observed for the non-PEG-coated AuNR system (Fig. SI-1). Moreover, the F C3H monolayer acquired stability before the HTC monolayer in contact with AuNR-PEG. Indeed, an initial surface pressure of 6 mN/m was observed for the F C3H monolayer as compared to 4 mN/m of surface pressure obtained for HTC. Fig. 5(a) shows that the molecular area of the F C3H monolayer decreased to at least 60 $Å^2$ at 15 mN/m, behavior that is similar to that observed in the previous system. The zeta potential value of the subphase showing a value of −4.77 mV, lower when compared to the zeta potential of AuNR-PEG +9.66 mV. A similar interaction is also obseved for HTC monolayer (zeta potential value of −7.67 mV). AuNR-PEG had a greater influence on the HTC monolayer, with an increase of 30 $Å^2$ in molecular area at 10 mN/m compared to 5 $Å^2$ for positive AuNPs or AuNRs at the same pressure.

The binding energy of the membrane samples and nanomaterials was determined by the thermodynamic parameters obtained by ITC measurements and AFM phase images were used to confirm these interactions. Representative titration curves and AFM phase images of F C3H and HTC binding with AuNRs-PAH are shown in Fig. 6.

The AuNRs-PAH were titrated in a buffered solution and no significant heat was released or absorbed (Fig. SI-4). It is important to emphasize the concentrations of the extracted membranes cannot be accurately determined and, therefore, we report here the thermodynamic trends. Raw data from the titration of AuNR-PEG into the extracted membranes showed no interaction [see Fig. SI-5(a)], which is probably due the low surface charge and wettability of PEG molecules, which creates a barrier of water molecules, hindering the interaction [28,29]. AFM phase images confirmed the absence of interaction as both membranes maintained most of their original conformation [Fig. SI-5 (b)].

Contrarialy, when AuNRs-PAH are titrated into F C3H or HTC membrane samples [Fig. 6(a) and (d)], significant endothermic peaks followed by small exothermic peaks are observed. This kind of ITC thermogram is not typical, and it can be attributed to the heterogeneity of the samples. The saturation is delayed for both exothermic and endothermic peaks in the HTC thermogram compared to the F C3H. These thermodynamic differences were visible in the AFM phase images taken before and after the titration measurements. When AuNR was added to the F C3H sample, the vesicle domains initially observed in Fig. 6(b) were broken [Fig. 6(c)]. On the other hand, for HTC vesicles, a reduction in their size after the AuNR titration, followed by an aggregation process, are observed as shown in Fig. 6(e) and (f).

4. Discussion

The organization of the lipids extracted from healthy and cancerous cells as monolayers was evaluated. The choice of cells was based on differences in their lipid composition, that is, cancer cell membranes are known to be more hydrophilic because of the glycolipids in their structure as compared to the healthy ones [25]. The results reveal a significant difference in composition between healthy cell membranes and cancerous ones, which in turn can influence their stability in solution and in a subphase. The literature reports the existence of larger

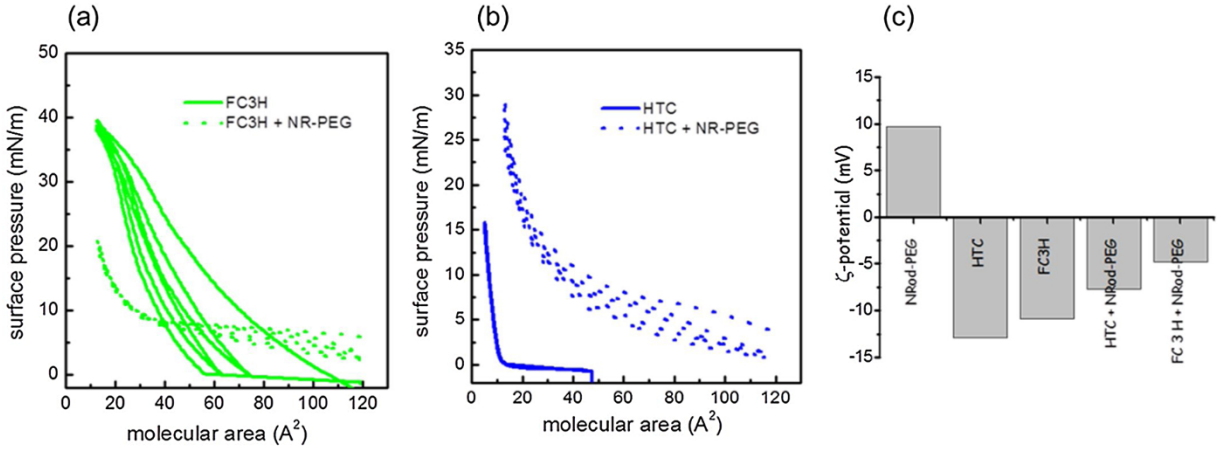

Fig. 5. Surface pressure–area isotherms of (a) F C3H and (b) HTC monolayers with ~10^9 particles/mL of AuNR-PEG in the subphase. (c) Zeta potential values obtained from the subphase of the Langmuir trough containing nanoparticles after compression of the monolayer.

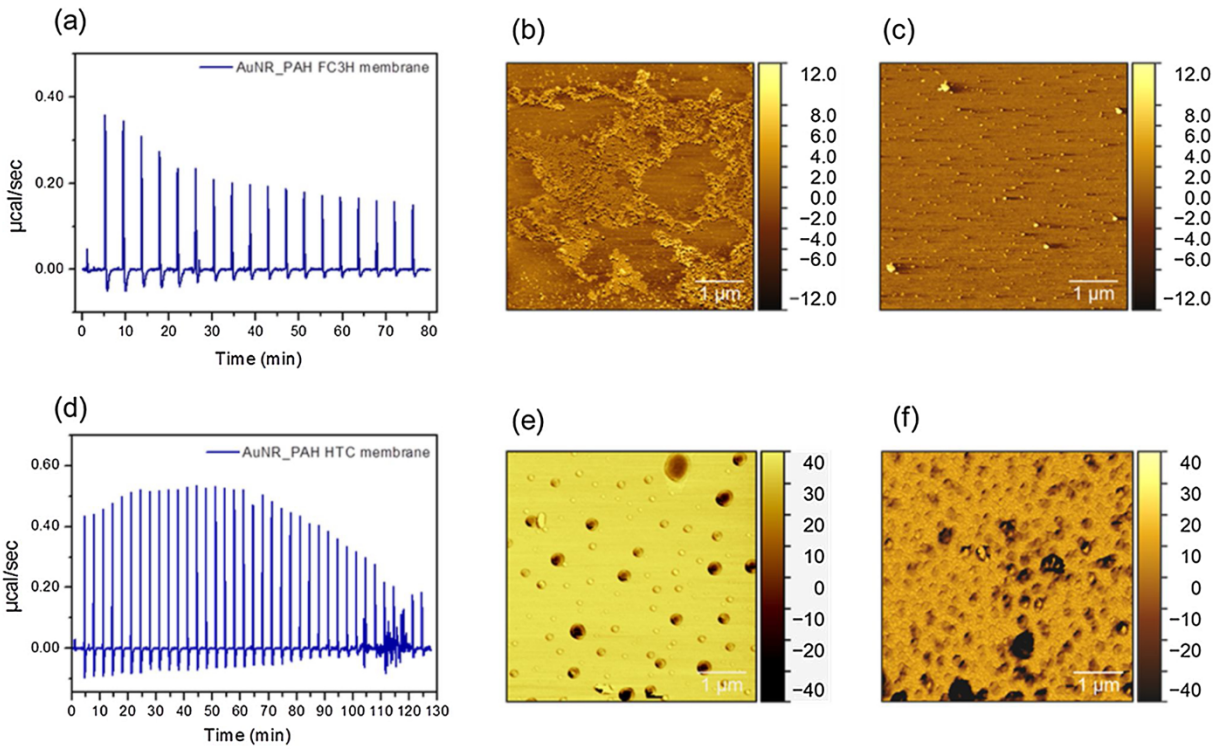

Fig. 6. ITC raw data from the titration of AuNR into (a) F C3H and (d) HTC membrane samples. The ITC experiments were conducted in 1 mM tris−HCl buffer at pH = 7.4. AFM phase images of the membrane samples F C3H and HTC (b,e) before and (c,f) after the titration of AuNR.

amounts of carbohydrate residues in cancer cell membranes, which can create asymmetry in the cell membrane. These same residues can create an extra layer that covers the outer surface of the membrane, which changes the surface charge and membrane fluidity [31]. The planar chromatography results showed a prevalence of nonpolar lipids in the F C3H membrane sample. These types of lipids can create an apolar environment on the membrane surface as compared to the HTC sample lipids. The surface charge difference between both membranes is also reflected in the zeta potential values: −10.9 mV for F C3H and −12.9 mV for HTC. According to previous results, there are significant differences in the electrical charge and lipid composition of healthy and cancerous cells due to the outer layer of carbohydrate residues in this last one, which can change the charge by 1 or 2 mV[13]. Moreover, cancerous cells also present a mass ratio of phosphatidylcholine and phosphatidylethanolamine phospholipids higher than the healthy ones. The latter was observed in our results, which showed 74 % phospholipids in the cancerous cells as compared to 62 % in the healthy ones. Differences in membrane composition can result in serious metabolic disturbances. For example, an increase in the number of phospholipid molecules in the cell membrane results in an increased number of amino, carboxyl, and phosphate groups, which can change the pH of the environment near the cell [32].

F C3H monolayer showed a well-defined isotherm profile with an increased surface pressure activity along the molecular area and a transition phase around 30 Å^2. The latter can be attributed to the presence of double bonds in some lipid and phospholipid molecules of the membrane, which could result in lower cohesion between the carbon chains, typical in synthetic lipids. In the molecular area around 40 Å^2, a transition phase is observed for the F C3H monolayer and it is similar to the transition phase between the gaseous and cohesion states. According to Langmuir theory's, this is a typical monolayer that behaves as a duplex film in which the polar end groups are in a two-dimensional state, whereas the attractive forces between the carbon chains retain a cohesive monolayer [33,34].

In contrast, the HTC monolayer presents a profile close to the expanded–condensed liquid phase, without any transition phase. This can be related to the smaller number of apolar lipids in the HTC membrane as compared to the F C3H sample. Moreover, the number of hydrophilic molecules, for example, sugars or carbohydrates, could make this monolayer more oriented to the aqueous subphase, as illustrated in Fig. 3(d) and (e). Compression–decompression cycles were performed to assess how the F C3H and HTC membranes behave across a physical disorder. The loss of stability during cycling suggests that the F C3H monolayer was becoming a vesicle, leaving the interface to the subphase. Although F C3H was unstable during cycling, the F C3H isotherms had an uniform profile in terms of surface pressure as a function of molecular area. With respect to the HTC monolayer, it showed stable performance over the compression–decompression cycles; that is, the monolayer formed by the HTC membrane remained stable at the air–water interface and did not exhibit any hysteresis.

A significant difference in the surface pressure was observed when AuNPs or AuNRs were added to the subphase. Two distinguishing behaviors for the HTC and F C3H monolayers in the presence of AuNPs or AuNRs were observed. The F C3H monolayer isotherms - in the presence of both AuNPs and AuNRs - showed a decrease of almost 60 Å^2 to a smaller molecular area. The two possible explanations are:

i) AuNPs and AuNRs may induced condensation of the monolayer, *i.e.*, at a given pressure, such as 10 mN/m, fewer molecules remained per area as compared to the F C3H monolayer without nanomaterials. According to Davis, this is known as a threshold area, when the molecular forces remain small for each molecule [34]. In this case, the area decreased because the monolayer was almost in a solid state. A possible explanation is the existence of islands between the lipid molecules and nanoparticles in the subphase, resulting in strong cohesion between the hydrocarbon chains;

ii) Another hypothesis is the formation of vesicles composed by phospholipds (from the monolayer) and nanoparticles, that can migrate from the interface to the subphase, as illustrated by Fig. 3(d) and (e). In this case, the monolayer–nanoparticle interaction is strong enough to allow the formation of an F C3H bilayer around the AuNRs and AuNPs.

Moreover, the remaining lipids can be organized as a condensed monolayer that is almost solid. The zeta potential values obtained for F C3H/AuNR and F C3H/AuNP systems is an indicative of vesicles formation, as shown in Fig. 4(c). Comparing the AuNR zeta potential values, a variation of values from +35 mV to +29 mV in the presence of F C3H membranes was observed. This decrease may be associated with a negative "extra layer" around the AuNRs, which is acceptable since the zeta potential value of the F C3H membrane was −11 mV. The same behavior was observed for the interaction between the F C3H monolayer and the AuNPs. There was a decrease in the zeta potential value of this system from +37 mV to +30 mV. Fig. 4(d) and (e) show illustrations of these interactions.

On the other hand, the AuNP and AuNR particles induced a shift in the HTC monolayer for large molecular areas of at least 6 $Å^2$ and to a surface pressure of 10 mN/m. In this case, there was probably some kind of interaction between the particles and the monolayer that allowed these increases in the molecular area values. Even with this interaction, the adsorption at the surface of the particles was also remarkable, as observed by the zeta potential values in Fig. 3(c). A reduction of the zeta potential value from +35 mV to +30 mV was found for the HTC/AuNR system and that from +37 mV to +23 mV was found for the HTC/AuNP system.

The compression–decompression curves with F C3H and HTC monolayers in presence of the nanoparticles showed no significant surface pressure or molecular area shift for AuNRs or AuNPs. It is interesting that both types of particles have the same behavior, indicating that the morphology did not have a significant impact on this kind of interaction; only the membrane composition affected the results. Therefore, differences in morphology – spherical or rod shape – did not have a significant influence on the bio-nano interface, as observed in Fig. 4(a) and (b). The charge influence of those particles were investigated using the PEG functionalization that has been extensively used to extend the *in vivo* blood circulation time of particles and to improve their passive and active accumulation in tumors [35]. This investigation suggests that AuNR-PEG has significant interaction with the F C3H membrane. The hypothesis is that the interaction of the F C3H monolayer with the AuNR-PEG resulted in the formation of vesicles and that the remaining lipid molecules at the interface formed a condensed, almost solid monolayer, as revealed by our zeta potential values. HTC monolayer became less stable with AuNR-PEG because of variations in the compression–decompression cycles. It is interesting that the F C3H and HTC monolayers had similar isotherm results for AuNRs, AuNPs, and AuNR-PEG. However, AuNR-PEG present greater influence on the HTC monolayer, indicating that the surface charge had more influence on the bio-nano interface when compared to the morphology.

The binding of membrane samples and nanomaterials was determined by the thermodynamic parameters obtained by ITC measurements, and confirmed by AFM images. In both systems, the exothermic peak can be related to the electrostatic attraction that overcomes the solvation layer of water molecules, whereas the endothermic peak can be related to the movement of water molecules and the rearrangement of lipids [28]. HTC has more proteins and consequently more sites of interactions with the nanorods as compared to F C3H. Therefore, F C3H saturation occurred earlier because of the absence of sites to interact. The Langmuir results showed the same trends. The change in the isotherm profile of the F C3H monolayer was related to the high lipid content, causing packed domains when in contact with the AuNRs. The expansion that occurred in the HTC monolayer with AuNRs was related to the high polarity and the attraction between the particles. The isotherms of HTC with AuNR-PEG systems showed more expansion as compared to HTC with AuNRs because of the PEG wettability, which goes to the interface with molecules of water. However, there was no interaction in ITC experiments with AuNR-PEG because the water movement was not energetically favored in solution.

5. Conclusion

In summary, we can state from the results discussed herein that AuNRs, AuNPs, and AuNR-PEG significantly altered the organization of reconstituted F C3H and HTC membranes as monolayers. For F C3H membranes, in particular, the nanoparticles tended to carry the membrane into the solution, causing dissolution of the monolayer, and the remaining monolayer was shown to be highly organized into domains. The results suggested that the nanoparticles altered the packing of the F C3H lipids, forming a bilayer into the subphase. A similar phenomenon was observed for HTC monolayer, but the nanoparticles were still able to interact with the membrane, thus expanding the monolayers. These results mean that initially there is an adsorption of nanoparticles on the surfaces of the cells because of the interaction with the lipids, leading to further incorporation. Furthermore, the differences in terms of the hydrophilic or hydrophobic behavior of each membrane were fundamental to these interactions. This study model using real membrane showed that the major limitant for this interaction is the membrane composition and the nanoparticle functionalization, not the nanomaterial shape.

Declaration of Competing Interest

The authors declare that they have no known competing financial interests or personal relationships that could have appeared to influence the work reported in this paper.

Acknowledgments

The authors are grateful to FAPESP, CAPES and CNPq for the financial assistance. JC-B thanks FAPESP process 2012/03570-0 and 2016/14303-3, PMPL thanks FAPESP process 2012/15630-7 and VSM thanks FAPESP 2012/11166-4. The authors thank LME/LNNano for technical support during the electron microscopy.

Appendix A. Supplementary data

Supplementary material related to this article can be found, in the online version, at doi:https://doi.org/10.1016/j.mtcomm.2020.101831.

References

[1] A. Lesniak, A. Salvati, M.J. Santos-Martinez, M.W. Radomski, K.A. Dawson, C. Aberg, Nanoparticle adhesion to the cell membrane and its effect on nanoparticle uptake efficiency, J. Am. Chem. Soc. 135 (4) (2013) 1438–1444.
[2] C. Corredor, W.-C. Hou, S.A. Klein, B.Y. Moghadam, M. Goryll, K. Doudrick, P. Westerhoff, J.D. Posner, Disruption of model cell membranes by carbon nanotubes, Carbon 60 (2013) 67–75.
[3] M. Lelimousin, M.S.P. Sansom, Membrane perturbation by carbon nanotube insertion: pathways to internalization, Small 9 (21) (2013) 3639–3646.
[4] C. Peetla, V. Labhasetwar, Biophysical characterization of nanoparticle-endothelial model cell membrane interactions, Mol. Pharm. 5 (3) (2008) 418–429.
[5] A. Nel, T. Xia, H. Meng, X. Wang, S.J. Lin, Z.X. Ji, H.Y. Zhang, Nanomaterial toxicity testing in the 21st century: use of a predictive toxicological approach and high-throughput screening, Acc. Chem. Res. 46 (3) (2013) 607–621.
[6] G. Oberdorster, Safety assessment for nanotechnology and nanomedicine: concepts of nanotoxicology, J. Intern. Med. 267 (1) (2010) 89–105.
[7] L.C. Cheng, X.M. Jiang, J. Wang, C.Y. Chen, R.S. Liu, Nano-bio effects: interaction of nanomaterials with cells, Nanoscale 5 (9) (2013) 3547–3569.
[8] N. Li, P. Zhao, D. Astruc, Anisotropic gold nanoparticles: synthesis, properties, applications, and toxicity, Angewandte Chem. Int. Ed. 53 (7) (2014) 1756–1789.
[9] P. Rivera-Gil, D.J. De Aberasturi, V. Wulf, B. Pelaz, P. Del Pino, Y. Zhao, J. Y.; De La Fuente, I.R. M.; De Larramendi, T. Rojo, X.J. Liang, W.J. Parak, The challenge to relate the physicochemical properties of colloidal nanoparticles to their cytotoxicity, Acc. Chem. Res. 46 (3) (2013) 743–749.
[10] P. Rivera Gil, G. Oberdoerster, A. Elder, V. Puntes, W.J. Parak, Correlating physicochemical with toxicological properties of nanoparticles: the present and the future, ACS Nano 4 (10) (2010) 5527–5531.
[11] M.L. Berkowitz, R. Vacha, Aqueous solutions at the interface with phospholipid bilayers, Acc. Chem. Res. 45 (1) (2012) 74–82.
[12] M.N. Christiansen, J. Chik, L. Lee, M. Anugraham, J.L. Abrahams, N.H. Packer, Cell surface protein glycosylation in cancer, Proteomics 14 (4-5) (2014) 525–546.

[13] I. Dobrzynska, E. Skrzydlewska, Z.A. Figaszewski, Changes in electric properties of human breast Cancer cells, J. Membr. Biol. 246 (2) (2013) 161–166.
[14] B. Szachowicz-Petelska, I. Dobrzynska, S. Sulkowski, Z. Figaszewski, Characterization of the cell membrane during cancer transformation, J. Environ. Biol. 31 (5) (2010) 845–850.
[15] H. Lis, N. Sharon, Lectins: Carbohydrate-specific proteins that mediate cellular recognition, Chem. Rev. 98 (2) (1998) 637–674.
[16] I. Dobrzynska, E. Skrzydlewska, Z. Figaszewski, Parameters characterizing acid-base equilibria between cell membrane and solution and their application to monitoring the effect of various factors on the membrane, Bioelectrochemistry 69 (2) (2006) 142–147.
[17] I. Dobrzynska, B. Szachowicz-Petelska, B. Darewicz, Z.A. Figaszewski, Characterization of human bladder cell membrane during Cancer transformation, J. Membr. Biol. 248 (2) (2015) 301–307.
[18] P.R. Leroueil, S.Y. Hong, A. Mecke, J.R. Baker, B.G. Orr, M.M.B. Holl, Nanoparticle interaction with biological membranes: Does nanotechnology present a janus face? Acc. Chem. Res. 40 (5) (2007) 335–342.
[19] C. Peetla, V. Labhasetwar, Effect of molecular structure of cationic surfactants on biophysical interactions of surfactant-modified nanoparticles with a model membrane and cellular uptake, Langmuir 25 (4) (2009) 2369–2377.
[20] J. Cancino, T.M. Nobre, O.N. Oliveira Jr., S.A.S. Machado, V. Zucolotto, A new strategy to investigate the toxicity of nanomaterials using Langmuir monolayers as membrane models, Nanotoxicology 7 (1) (2013) 61–70.
[21] G. Rossi, J. Barnoud, L. Monticelli, Polystyrene nanoparticles perturb lipid membranes, J. Phys. Chem. Lett. 5 (1) (2014) 241–246.
[22] J. Cancino, I.M.M. Paino, K.C. Micocci, H.S. Selistre-de-Araujo, V. Zucolotto, In vitro nanotoxicity of single-walled carbon nanotube-dendrimer nanocomplexes against murine myoblast cells, Toxicol. Lett. 219 (1) (2013) 18–25.
[23] T.M. Uehara, V.S. Marangoni, N. Pasquale, P.B. Miranda, K.-B. Lee, V. Zucolotto, A detailed investigation on the interactions between magnetic nanoparticles and cell membrane models, ACS Appl. Mater. Interfaces 5 (24) (2013) 13063–13068.
[24] C. Peetla, S.H. Jin, J. Weimer, A. Elegbede, V. Labhasetwar, Biomechanics and thermodynamics of nanoparticle interactions with plasma and endosomal membrane lipids in cellular uptake and endosomal escape, Langmuir 30 (25) (2014) 7522–7532.
[25] C. Peetla, S. Vijayaraghavalu, V. Labhasetwar, Biophysics of cell membrane lipids in cancer drug resistance: implications for drug transport and drug delivery with nanoparticles, Adv. Drug Deliv. Rev. 65 (13–14) (2013) 1686–1698.
[26] R. Palankar, B.E. Pinchasik, B.N. Khlebtsov, T.A. Kolesnikova, H. Mohwald, M. Winterhalter, A.G. Skirtach, Nanoplasmonically-induced defects in lipid membrane monitored by ion current: transient nanopores versus membrane rupture, Nano Lett. 14 (8) (2014) 4273–4279.
[27] R. Lund, R. Leth-Larsen, O.N. Jensen, H.J. Ditzel, Efficient isolation and quantitative proteomic analysis of Cancer cell plasma membrane proteins for identification of metastasis-associated cell surface markers, J. Proteome Res. 8 (6) (2009) 3078–3090.
[28] D.F. Moyano, M. Ray, V.M. Rotello, Nanoparticle-protein interactions: water is the key, MRS Bull. 39 (12) (2014) 1069–1073.
[29] C.C. You, M. De, V.M. Rotello, Contrasting effects of exterior and interior hydrophobic moieties in the complexation of amino acid functionalized gold clusters with alpha-chymotrypsin, Org. Lett. 7 (25) (2005) 5685–5688.
[31] T. Lange, T.R. Samatov, A.G. Tonevitsky, U. Schumacher, Importance of altered glycoprotein-bound N- and O-glycans for epithelial-to-mesenchymal transition and adhesion of cancer cells, Carbohydr. Res. 389 (2014) 39–45.
[32] B. Szachowicz-Petelska, I. Dobrzynska, M. Skrodzka, B. Darewicz, Z. A. Figaszewski, J. Kudelski, Phospholipid composition and electric charge in healthy and cancerous parts of human kidneys, J. Membr. Biol. 246 (5) (2013) 421–425.
[33] M.C. Petty, Langmuir-Blodgett Films: An Introduction, Cambridge University Press, Cambridge, 1996.
[34] J.T. Davies, E.K. Rideal, Interfacial Phenomena, Academic Press, Inc, London, 1961 p 480.
[35] D.E. Owens, N.A. Peppas, Opsonization, biodistribution, and pharmacokinetics of polymeric nanoparticles, Int. J. Pharm. 307 (1) (2006) 93–102.